

Multi-view Banded Spectral Clustering with application to ICD9 clustering

Luwan Zhang¹, Katherine Liao², Isaac Kohane³, Tianxi Cai¹

¹*Department of Biostatistics, Harvard T.H. Chan School of Public Health, Boston MA*

²*Division of Rheumatology, Brigham and Women's Hospital, Boston MA*

³*Department of Biomedical Informatics, Harvard Medical School, Boston MA*

June 28, 2022

Abstract

Despite recent development in methodology, community detection remains a challenging problem. Existing literature largely focuses on the standard setting where a network is learned using an observed adjacency matrix from a single data source. Constructing a shared network from multiple data sources is more challenging due to the heterogeneity across populations. Additionally, when a natural ordering on the nodes of interest arises, no existing method takes such information into account. Motivated by grouping the International classification of diseases, ninth revision, (ICD9) codes to represent clinically meaningful phenotypes, we propose a novel spectral clustering method that optimally combines multiple data sources while leveraging the prior ordering knowledge. The proposed method combines a banding step to encourage a desired moving average structure with a subsequent weighting step to maximize consensus across multiple sources. Its statistical performance is thoroughly studied under a multi-view stochastic block model. We also provide a simple rule of choosing weights in practice. The efficacy and robustness of the method is fully demonstrated through extensive simulations. Finally, we apply the method to the ICD9 coding system and yield a very insightful clustering structure by integrating information from a large claim database and two healthcare systems.

Key words: banding, multi-view, spectral clustering, stochastic block model

1 Introduction

The International Classification of Disease, 9th edition (ICD9) coding system, containing over 14,000 codes, is a widely adopted mechanism for billing. The ICD9 code information is also a valuable resource for research as it records a full spectrum of diagnoses and procedure information in the electronic health records (EHR). As a fundamental EHR constituent, the ICD9 coding system, although designed for billing and administrative functions, has been successfully used for many types of research (Kiyota et al., 2004; Klompas et al., 2008; Herzig et al., 2009, e.g.). However, individual ICD9 codes tend to be too specific to be directly used as disease phenotypes for research purposes. Many codes essentially describe the same disease and only differ in details such as the anatomical areas affected. For clinical and genetic studies, it is thus often desirable to collapse detailed codes into clinically relevant groups.

To address such a need, Denny et al. (2010, 2013) manually curated grouping information to allow for more efficient representation of disease phenotypes recorded in the EHR. The grouping has been successfully used to perform phenome-wide association studies (PheWAS) where the goal is to associate a genetic variant to a wide range of disease phenotypes. The current PheWAS grouping is no doubt a valuable asset to the research community. However, the manual curation approach has major limitations including lack of scalability, portability and susceptible to subjective bias. With the adoption of ICD10 codes in recent years, a substantial human effort will be required to manually update the grouping to include both ICD9 and ICD10 codes. This signifies the need for a data-driven approach to grouping the ICD codes. In this paper, we propose a data-driven clustering approach to grouping the ICD codes, combining information from multiple EHR and claims data sources. The proposed approach has the advantage of being efficient, scalable, and adaptive to the evolving human knowledge as reflected in the observed data.

We translate the problem of grouping ICD codes with multiple, say m , data sources to a statistical problem of constructing a network based on m different observed similarity matrices. Network analysis has been an active area of research in recent years with a range of methods available, see (Newman, 2006; Bickel and Chen, 2009; Zhao et al., 2012, e.g.). One class of methods that has

gained much popularity is based on spectral clustering, (Shi and Malik, 2000; Ng et al., 2002, e.g.), in part due to their superior empirical performance and supported theoretical justifications. Given a graph $\mathbb{G} = (\mathcal{V}, \mathbb{A})$, where $\mathcal{V} = \{v_i\}_{i=1}^n$ represents the vertex set and \mathbb{A} is the observed adjacency matrix, spectral clustering performs a spectra analysis either directly on \mathbb{A} or its Laplacian and applies the k-means to seek a partition such that

$$\mathcal{V} = \cup_k \mathcal{V}_k, \mathcal{V}_k \cap \mathcal{V}_l = \emptyset, \forall k \neq l.$$

In addition to being fast and simple to implement, spectral clustering has been shown to possess good statistical properties under the framework of stochastic block model (SBM) (Holland et al., 1983) and its extension to allow for degree heterogeneity (Karrer and Newman, 2011; Rohe et al., 2011; Qin and Rohe, 2013; Lei et al., 2015; Jin et al., 2015, e.g.).

One limitation of these methods is that only a single adjacency matrix \mathbb{A} is considered for estimating the graph structure. When multiple adjacency matrices from different data sources are available, multi-view clustering methods have been proposed (Blaschko and Lampert, 2008; Chaudhuri et al., 2009; Cai et al., 2011; Kumar and Daumé, 2011; Xia et al., 2014, e.g.). Despite their empirical success, little theoretical justifications are provided until recently Han et al. (2014) and Paul et al. (2016) showed some consistency results. However, all these methods require input being unweighted, binary-valued adjacency matrices, which would largely hamper the applicability to settings with similarity matrices being weighted and real-valued as in our motivating example of clustering ICD9 codes. Real-valued measures of similarity are used frequently in biological and clinical applications. With the recent emergence of *word2vec* algorithms (Mikolov et al., 2013 a), biological sequences (e.g. genes, proteins), clinical concepts describing disease conditions, and ICD9 codes have been represented by Euclidean vectors (Asgari and Mofrad, 2015; Nguyen et al., 2016; Choi et al., 2016; Ng, 2017, e.g.), in which case a cosine similarity is often used to summarize pairwise similarity. In our motivating example, another important feature is that there is a natural ordering to the ICD9 codes such that codes further apart are less likely to belong to the same group. Such natural ordering occurs in other biological examples as well, for example when nodes represent chromosomal loci, clusters of homogeneous genes tend to be adjacent genes (Hurst et al., 2004).

Conventional clustering methods may not be efficient since they simply ignore such valuable prior information.

To the best of our knowledge, no existing clustering method incorporates multiple real-valued similarity matrices with ordered nodes. In this paper, we propose a novel multi-view banded spectral clustering (mvBSC) method to optimally combine information from multiple sources and leverage the ordering information. The rest of paper is organized as follows. In Section 2, we give a formal description of the multi-view stochastic block model for ordered nodes. Section 3 details the proposed multi-view banded spectral clustering method and provides theoretical justifications under the multi-view stochastic block model. Simulations are given in Section 4 to demonstrate the efficacy and robustness of the proposed method. Section 5 presents thorough data analysis on ICD9 codes clustering. Concluding remarks and discussions are given in Section 6.

2 Multi-view Stochastic Block Model for Ordered Nodes

2.1 Notations

For any matrix $\mathbb{A} \in \mathcal{R}^{p \times p}$, let \mathbb{A}_i and $\mathbb{A}_{\cdot i}$ respectively denote the i th row and column of \mathbb{A} , and let $\|\mathbb{A}\|_F$ and $\|\mathbb{A}\|$ respectively denote its Frobenius norm and spectral norm. For any two matrices $\mathbb{A}, \mathbb{B} \in \mathcal{R}^{p \times p}$, $\mathbb{A} \lesssim \mathbb{B}$ means that $\mathbb{A} \leq c\mathbb{B}$ for some constant $c > 0$ and $\mathbb{A} \gtrsim \mathbb{B}$ means that $\mathbb{A} \geq c\mathbb{B}$ for some constant $c > 0$. $\mathbb{A} \asymp \mathbb{B}$ is equivalent as $\mathbb{A} \lesssim \mathbb{B} \lesssim \mathbb{A}$. For any vector $\mathbf{a} = (a_1, \dots, a_p)^\top$, let $\text{diag}(\mathbf{a})$ denote the corresponding $p \times p$ diagonal matrix with diagonals being \mathbf{a} and $\|\mathbf{a}\|_2$ be its ℓ_2 -norm. Let $\mathbf{1}_p = (1, \dots, 1)^\top$ denote the all-one vector in \mathcal{R}^p and $\mathbf{a} \geq 0$ indicate the coordinatewise non-negativity. For $x, y \in \mathcal{R}$, $x = o(y)$ means $\frac{x}{y} = o(1)$. Let $I(\cdot)$ denote the indicator function.

Suppose the data for analysis consist of m similarity matrices, $\{\mathbb{W}^s, s = 1, \dots, m\}$, representing m undirected weighted graphs, $\mathbb{G}^s = \{\mathcal{V}, \mathbb{W}^s\}$, where $\mathbb{W}^s = [W_{ij}^s]_{n \times n}$, W_{ij}^s is the similarity between the nodes v_i and v_j based on the s th view, and we assume that these m graphs share the same vertex set $\mathcal{V} = \{v_i\}_{i=1}^n$ which has a non-overlapping K -partition network structure

$$\mathcal{V} = \{\cup_{k=1}^K \mathcal{V}_k, \mathcal{V}_k \cap \mathcal{V}_l = \emptyset, \forall 1 \leq k < l \leq K\},$$

where $\mathcal{V}_k = \{v_i\}_{i:g_i=k}$ and $g_i \in \{1, \dots, K\}$ indexes which group v_i belongs to. The partition can also be represented by a group membership matrix

$$\mathbb{Z}^* = [\mathbb{Z}_{ik}^*]_{n \times K} \in \mathcal{Z}_{n,K}, \quad \text{where} \quad \mathbb{Z}_{ik}^* = I(v_i \in \mathcal{V}_k) = I(g_i = k),$$

and $\mathcal{Z}_{n,K}$ consists of all possible K -group membership matrices for n nodes. Denote its associated class of projector matrices by

$$\mathcal{P}_{n,K} = \left\{ \mathbb{Z} [\text{diag}(\mathbf{1}_n^\top \mathbb{Z})]^{-1} \mathbb{Z}^\top : \mathbb{Z} \in \mathcal{Z}_{n,K} \right\}$$

In particular, denote by $P_{\mathbb{Z}}$ the projector matrix $\mathbb{Z} [\text{diag}(\mathbf{1}_n^\top \mathbb{Z})]^{-1} \mathbb{Z}^\top$ that projects any n -dimensional vector to the K -dimensional subspace spanned by the columns of \mathbb{Z} . Throughout, we assume that K is known and remains as a constant for all theoretical analyses. Strategies for choosing K in practice will be discussed in Section 5.

2.2 Assumptions on mvSBM and Node Ordering

We aim to optimally combine information from the m -views, $\{\mathbb{W}^s = [W_{ij}^s]_{n \times n}, s = 1, \dots, m\}$, to learn about the network structure through an mvSBM such that $\forall 1 \leq i < j \leq n$,

$$\mathbb{E}_{\mathbb{Z}^*} W_{ij}^s \equiv \mathcal{W}_{ij}^s = \Omega_{g_i g_j}^s, \quad \mathcal{W}^s = [\mathcal{W}_{ij}^s]_{i=1, \dots, n}^{j=1, \dots, n} = \mathbb{Z}^* \Omega^s \mathbb{Z}^{*\top}, \quad |W_{ij}^s| \leq L, \quad \text{Var}_{\mathbb{Z}^*}(W_{ij}^s) = \sigma_s^2, \quad (2.1)$$

where $\Omega^s = [\Omega_{kl}^s]_{k=1, \dots, K}^{l=1, \dots, K} \in [-L, L]^{K \times K}$ is a symmetric and positive definite matrix of rank K , $L < \infty$ is a constant, $\mathbb{E}_{\mathbb{Z}^*}$ and $\text{Var}_{\mathbb{Z}^*}$ respectively denote the expectation and variance given the membership matrix \mathbb{Z}^* . Thus, under the mvSBM, the hidden membership matrix \mathbb{Z}^* is shared across all m views, but the connection intensities encoded by Ω^s may vary. For each diagonal element W_{ii}^s , it can be either considered as a yet another independent bounded random variable following the model specified in (2.1), or it can be treated as a non-random constant $\omega_0 \in [-L, L]$. Without loss of generality, we consider hereafter the latter case, which includes most commonly used similarity measures.

Remark 1. *The traditional definition of a SBM given in Holland et al. (1983) requires that each \mathbb{W}^s is 0/1 valued in that each off-diagonal entry corresponds to an independent Bernoulli random*

variable whose probability depends only on the block memberships of the two nodes. Here we extend to a real-valued setting to allow for more generality. In fact, Karrer and Newman (2011) was the first attempt to extend the applicability of a SBM in which a Poisson model is imposed to allow for multiple edges between any two nodes.

In our motivating example, the nodes obey a natural ordering in that ICD codes further apart in “distance” are less likely to be grouped together. To incorporate such valuable ordering information to the underlying model, we introduce a pre-defined distance metric $d : \mathcal{V} \times \mathcal{V} \mapsto [0, \infty)$, which satisfies the well-known non-negativity, symmetry and identity property: $\forall (v_i, v_j) \in \mathcal{V} \times \mathcal{V}$,

$$d(v_i, v_j) \geq 0, \quad d(v_i, v_j) = d(v_j, v_i), \quad d(v_i, v_j) = 0 \Leftrightarrow v_i = v_j$$

However, the triangle inequality is not required. In the following, d_{ij} will also be used to express $d(v_i, v_j)$ for brevity. For example, \mathcal{V} denotes all strings of ICD9 codes and the pairwise distance can be obtained through their numerical representations, e.g., $d(\text{“331.1”}, \text{“331.9”}) = |331.1 - 331.9| = 0.8$. For $k = 1, \dots, K$, we define the centroid node of the cluster \mathcal{V}_k as v_{c_k} , where

$$c_k := \min \left\{ i : \operatorname{argmin}_{v_i \in \mathcal{V}_k} \sum_{v_j \in \mathcal{V}_k} d_{ij} \right\}$$

and $n_k := |\mathcal{V}_k|$ is the cardinality of \mathcal{V}_k . Then $\min_{v_i \in \mathcal{V}_k} i \leq c_k \leq \max_{v_i \in \mathcal{V}_k} i$.

To leverage the prior knowledge that nodes further apart are less likely to belong to the same group, we assume that

$$(C1) \text{ There exists a constant } \delta > 0 \text{ such that } d(v_i, v_{c_k}) \leq \delta, \quad \forall v_i \in \mathcal{V}_k, \quad k = 1, \dots, K.$$

Hence 2δ characterizes each cluster length. Without loss of generality, we further assume $\delta > d_0 := \min_{1 \leq i < j \leq n} d_{ij}$ which is naturally satisfied provided $K < n$. Assumption (C1) essentially enables us to employ banding on a similarity matrix with a bandwidth 2δ . Furthermore, we assume that the magnitude of $\Omega_{g_i g_j}^s$ shall vanish as c_{g_i} and c_{g_j} become more and more distant and hence consider

each Ω^s reside in the following restricted class of matrices, inspired by Bickel and Levina (2008),

$$\mathcal{F}_{\alpha_s} := \mathcal{F}(\alpha_s, L, \beta) = \left\{ \mathbb{O} = [O_{kl}]_{k=1, \dots, K}^{l=1, \dots, K} \in [-L, L]^{K \times K} : \mathbb{O} = \mathbb{O}^\top, \max_k \sum_{l: d(v_{c_k}, v_{c_l}) > h} |O_{kl}| \leq Lh^{-\alpha_s}, \right. \\ \left. h > 0, 0 < \beta \leq \gamma_K(\mathbb{O}) \leq \gamma_1(\mathbb{O}) \leq \beta^{-1} \right\} \quad (2.2)$$

where $\gamma_k(\mathbb{O})$ is k -th largest eigenvalue of \mathbb{O} , and $\alpha_s > 0$ controls the vanishing rate for off-diagonal entries as they move away from the diagonals. Intuitively, the larger α_s is, the easier to distinguish different communities. It is easy to see that $\alpha_1 < \alpha_2$ implies that $\mathcal{F}_{\alpha_2} \subset \mathcal{F}_{\alpha_1}$. Restriction of Ω^s on \mathcal{F}_{α_s} also leads to an immediate consequence on the parameter space of \mathcal{W}^s as described in Lemma 2.1, which loosely speaking is an expanded copy of \mathcal{F}_{α_s} , by the largest cluster size (Figure 2.1).

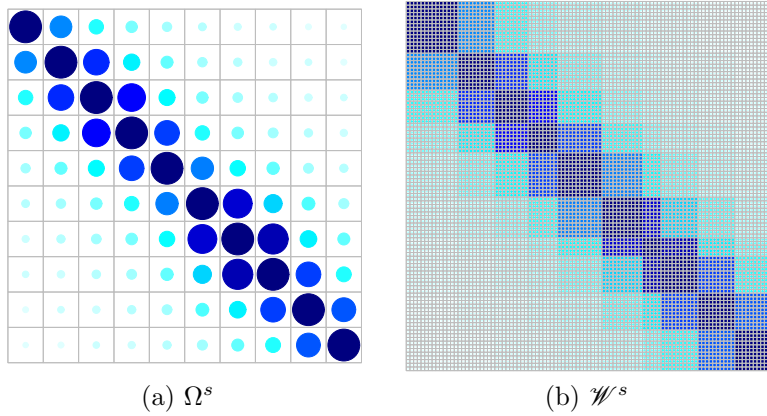


Figure 2.1: The left panel gives an example of the banding structure of Ω^s suggested in (2.2) and the right panel correspond to the structure of \mathcal{W}^s given in Lemma 2.1.

Lemma 2.1. *Suppose $\Omega^s \in \mathcal{F}_{\alpha_s}$ defined in (2.2) and \mathcal{V} satisfies condition (C1), given the membership matrix \mathbb{Z}^* , then $\mathcal{W}^s := \mathbb{Z}^* \Omega^s \mathbb{Z}^{*\top}$ resides in the following class of matrices*

$$\mathcal{H}_{\alpha_s} := \mathcal{H}(\alpha_s, \delta, L, \beta) = \left\{ \mathbb{A} = [A_{ij}]_{i=1, \dots, n}^{j=1, \dots, n} \in [-L, L]^{n \times n} : \mathbb{A} = \mathbb{A}^\top, \max_i \sum_{j: d(v_i, v_j) > h} |A_{ij}| \leq L n_{max} (h - 2\delta)^{-\alpha_s}, \text{ for all } h > 2\delta, \text{ and } 0 < n_{min} \beta \leq \gamma_K(\mathbb{A}) \leq \gamma_1(\mathbb{A}) \leq n_{max} / \beta \right\} \quad (2.3)$$

where $n_{min} = \min_k n_k, n_{max} = \max_k n_k$.

Figure 2.2 illustrates the concept of a centroid node v_{c_k} and the imposed cluster length.

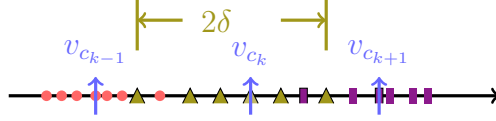


Figure 2.2: Nodes colored and symbolled in the same belong to the same group. Centroid nodes are highlighted by uparrows.

3 Multi-view banded spectral clustering (mvBSC)

In this section, we first summarize our proposed mvBSC procedure in Algorithm 1 and then give a brief explanation on the reasoning behind it. We then discuss the theoretical results supporting the validity and optimality of the proposed algorithm as well as the appropriate choices of the banding vector $\mathbf{h} = (h_1, \dots, h_m)^\top$ and the weight vector $\boldsymbol{\lambda} = (\lambda_1, \dots, \lambda_m)^\top$. Without loss of generality, we restrict our attention to the convex combination, $\boldsymbol{\lambda} \geq 0, \mathbf{1}_m^\top \boldsymbol{\lambda} = 1$.

3.1 The mvBSC procedure

The proposed mvBSC procedure is summarized as follows:

Input: m $n \times n$ similarity matrices $\mathbb{W}^1, \dots, \mathbb{W}^m$, number of groups K , a set of weight parameters $\lambda_1, \dots, \lambda_m \geq 0, \sum_{s=1}^m \lambda_s = 1$, and a set of banding parameters $h_1, \dots, h_m > 2\delta$

Output: Membership matrix $\widehat{\mathbb{Z}}^* \in \mathcal{L}_{n,K}$

for $s = 1:m$ **do**

- (1) $B_{h_s}(\mathbb{W}^s) := [\mathbb{W}_{ij}^s I(d_{ij} \leq h_s)]_{i=1, \dots, n}^{j=1, \dots, n} \leftarrow$ banding \mathbb{W}^s using the banding parameter h_s .
- (2) $\widehat{\mathbb{U}}^s \leftarrow$ the matrix of concatenating K eigenvectors corresponding to the first K largest absolute eigenvalues of $B_{h_s}(\mathbb{W}^s)$.

end

$\widehat{\mathbb{U}}_{\boldsymbol{\lambda}}^* \leftarrow$ the matrix of concatenating K eigenvectors corresponding to the first K largest eigenvalues of $\sum_{s=1}^m \lambda_s \widehat{\mathbb{U}}^s \widehat{\mathbb{U}}^{s\top}$.

Treating each row of $\widehat{\mathbb{U}}_{\boldsymbol{\lambda}}^*$ as a point in \mathcal{R}^K , run k-means to cluster these n points into K groups and obtain a corresponding membership matrix $\widehat{\mathbb{Z}}^*$.

Result: $\widehat{\mathbb{Z}}^*$

Algorithm 1: Multi-view banded spectral clustering (mvBSC)

Algorithm 1 involves two key steps: operating banding to each similarity matrix \mathbb{W}^s and performing spectral clustering on a convex combination of m projector matrices $\widehat{\mathbb{U}}^s \widehat{\mathbb{U}}^{s\top}$. To see the

reasoning, we first examine the eigen-space of \mathcal{W}^s . Let

$$\Delta = [\text{diag}(\mathbf{1}_n^\top \mathbb{Z}^*)]^{1/2} = \text{diag}(\sqrt{n_1}, \dots, \sqrt{n_K}), \quad \mathbb{U}^* = \mathbb{Z}^* \Delta^{-1},$$

and $\tilde{\Omega}^s := \Delta \Omega^s \Delta = [\Omega_{kl} \sqrt{n_k n_l}]_{k=1, \dots, m}^{l=1, \dots, m}$ with eigen-decomposition $\tilde{\Omega}^s = \mathbb{V}^s \mathbb{D}^s \mathbb{V}^{s\top}$. Then the eigen-decomposition of \mathcal{W}^s is given by

$$\mathcal{W}^s = \mathbb{U}^s \mathbb{D}^s \mathbb{U}^{s\top} = \mathbb{U}^* (\mathbb{V}^s \mathbb{D}^s \mathbb{V}^{s\top}) \mathbb{U}^{*\top}, \quad \text{where } \mathbb{U}^s = \mathbb{Z}^* \Delta^{-1} \mathbb{V}^s = \mathbb{U}^* \mathbb{V}^s.$$

Clearly, \mathbb{U}^s is a rotation of \mathbb{U}^* by \mathbb{V}^s and they correspond to the same K -dimensional subspace expressed by $P_{\mathbb{Z}^*} = \mathbb{U}^* \mathbb{U}^{*\top} = \mathbb{U}^s \mathbb{U}^{s\top}$. Since $(\Delta^{-1} \mathbb{V}^s)^{-1}$ exists, $\mathbb{U}_i^s = \mathbb{U}_j^s \Leftrightarrow g_i = g_j$, meaning that v_i and v_j are in the same group if and only if their corresponding rows in \mathbb{U}^s are the same. So the eigen-space of \mathcal{W}^s is membership structured and recovering \mathbb{U}^s is equivalent as recovering \mathbb{Z}^* .

Now consider the difference between \mathbb{W}^s and \mathcal{W}^s :

$$\mathbb{W}^s - \mathcal{W}^s = (\mathbb{W}^s - \mathbb{E}_{\mathbb{Z}^*} \mathbb{W}^s) + \text{diag}(\mathbb{E}_{\mathbb{Z}^*} \mathbb{W}^s - \mathcal{W}^s) = (\mathbb{W}^s - \mathbb{E}_{\mathbb{Z}^*} \mathbb{W}^s) + \text{diag}(\mathbb{W}^s - \mathcal{W}^s),$$

which is a symmetric bounded noise matrix plus a diagonal matrix. For the above equality, we note that $\text{diag}(\mathbb{W}^s) = \text{diag}(\mathbb{E}_{\mathbb{Z}^*} \mathbb{W})$ because the diagonals of \mathbb{W}^s are constants. Although the deviation from the eigenspace of \mathbb{W}^s to that of \mathcal{W}^s is always upper bounded by the operator norm of their difference, with no further information on the structure of \mathcal{W}^s , one can at most know the operator norm deviation is on the scale of \sqrt{n} since the noise matrix $(\mathbb{W}^s - \mathbb{E}_{\mathbb{Z}^*} \mathbb{W}^s)$ is on this scale and the remaining diagonal matrix can be treated as a constant and hence makes negligible contributions. Fortunately, Theorem 3.1 sheds light on the benefit of executing a banding operation that would enable us to significantly reduce the upper bound to the scale of $\sqrt{\log n} \max \left(\sqrt{\log n}, \left(\frac{n_{\max}}{\sqrt{\log n}} \right)^{\frac{1}{2\alpha_s+1}} \right)$ and this term shows explicitly the role of the decay parameter α_s in reducing the estimation error. Therefore, the space spanned by $\hat{\mathbb{U}}^s$ would show more resemblance to the space spanned by \mathbb{U}^* .

The other key step is the use of a weighted average $\sum_{s=1}^m \lambda_s \hat{\mathbb{U}}^s \hat{\mathbb{U}}^{s\top}$ to estimate $P_{\mathbb{Z}^*}$. Since each $\hat{\mathbb{U}}^s \hat{\mathbb{U}}^{s\top}$ can be viewed as a stand-alone estimator of $P_{\mathbb{Z}^*}$, $\hat{\mathbb{U}}^s \hat{\mathbb{U}}^{s\top}$ can be decomposed into $P_{\mathbb{Z}^*} + \mathbb{E}^s$, where \mathbb{E}^s is a symmetric error matrix. As an analogy of a weighted least square problem, to allow

for heterogeneity in noise corruptions, given a weight vector $\boldsymbol{\lambda}$, it is ideal to find

$$\widehat{\mathbb{Z}}_{\boldsymbol{\lambda}}^* = \operatorname{argmin}_{\mathbb{Z} \in \mathcal{Z}_{n,K}} \sum_{s=1}^m \lambda_s \|\widehat{\mathbb{U}}^s \widehat{\mathbb{U}}^{s\top} - P_{\mathbb{Z}}\|_F^2 \quad (3.1)$$

From a regularization perspective, these weights essentially put penalty on each view so that they can be dragged to a common ground expressed by $\widehat{\mathbb{Z}}_{\boldsymbol{\lambda}}^*$. However, the solution of (3.1) is NP-hard to find, and the alternative is to find the un-constrained solution $\sum_{s=1}^m \lambda_s \widehat{\mathbb{U}}^s \widehat{\mathbb{U}}^{s\top}$ as a surrogate whose eigenvectors can be subsequently used to reconstruct \mathbb{Z}^* .

In summary, the two sets of parameters \mathbf{h} and $\boldsymbol{\lambda}$ in the proposed mvBSC procedure play orthogonal but complementary roles. The banding parameter h_s maximally attempts to improve each individual performance, while the weight parameter λ_s allows for efficient message passing horizontally to make up each other's deficiencies.

3.2 Error analysis

To study the statistical performance of the proposed mvBSC procedure (Algorithm 1), it is important to realize that errors consist of two parts—distance from \mathbb{U}^* to $\widehat{\mathbb{U}}_{\boldsymbol{\lambda}}^*$ and the membership misallocation arising from the k-means step. The minimal distance between \mathbb{U}^* and $\widehat{\mathbb{U}}_{\boldsymbol{\lambda}}^*$ is equivalent to the distance between their respective subspace $P_{\mathbb{Z}^*}$ and $\widehat{\mathbb{U}}_{\boldsymbol{\lambda}}^* \widehat{\mathbb{U}}_{\boldsymbol{\lambda}}^{*\top}$ (Vu et al., 2013)

$$\frac{1}{2} \inf_Q \|\widehat{\mathbb{U}}_{\boldsymbol{\lambda}}^* - \mathbb{U}^* Q\|_F^2 \leq \|\widehat{\mathbb{U}}_{\boldsymbol{\lambda}}^* \widehat{\mathbb{U}}_{\boldsymbol{\lambda}}^{*\top} - P_{\mathbb{Z}^*}\|_F^2 \leq \inf_Q \|\widehat{\mathbb{U}}_{\boldsymbol{\lambda}}^* - \mathbb{U}^* Q\|_F^2 \quad (3.2)$$

where Q is a $K \times K$ orthonormal matrix. To evaluate the quality of the final k-means step, it is necessary to first define a “mis-clustered” node. To this end, recall that the k-means obtains

$$(\widehat{\mathbb{Z}}, \widehat{\mathbb{A}}) = \operatorname{argmin}_{\mathbb{Z} \in \mathcal{Z}_{n,K}, \mathbb{A} \in \mathcal{R}^{K \times K}} \left\| \widehat{\mathbb{U}}_{\boldsymbol{\lambda}}^* - \mathbb{Z} \mathbb{A} \right\|_F^2 \quad (3.3)$$

in which $\widehat{\mathbb{A}}_k^\top \in \mathcal{R}^K$ represents the k -th centroid (Steinhaus, 1956). Intuitively, if $\mathbb{U}_i^* Q$ is closer to $\widehat{\mathbb{A}}_{g_i}$ than it is to any other $\widehat{\mathbb{A}}_k$ for $k \neq g_i$, then node v_i can be correctly clustered.

Definition 1 (set of mis-clustered nodes). *Given $\mathbb{Z}^* \in \mathcal{Z}_{n,K}$, let $\mathbb{U}^* = \mathbb{Z}^* \Delta^{-1}$, $\widehat{\mathbb{U}}_{\boldsymbol{\lambda}}^*$ given in Algorithm 1, $\widehat{\mathbb{A}}$ defined in (3.3) and Q be a $K \times K$ orthonormal matrix satisfying (3.2), define $\mathcal{M}_{\boldsymbol{\lambda}}$ as*

the set of mis-clustered nodes

$$\mathcal{M}_\lambda = \left\{ i : \|\widehat{\mathbb{A}}_{g_i} - \mathbb{U}_i^* Q\|_2 \geq \sqrt{1/2n_{max}} \right\}$$

Remark 2. The definition of \mathcal{M}_λ is a sufficient condition to ensure $\|\widehat{\mathbb{A}}_{g_i} - \mathbb{U}_i^* Q\|_2 \leq \|\widehat{\mathbb{A}}_{g_j} - \mathbb{U}_j^* Q\|_2$ for any $g_j \neq g_i$, which was firstly considered in Rohe et al. (2011). The error analysis in this paper mainly addresses the global optimum of (3.3), and this optimization problem could suffer from local optima in practice.

Theorem 3.1 (optimal choice of banding parameter h). Given the membership matrix $\mathbb{Z}^* \in \mathcal{L}_{n,K}$, suppose a similarity matrix $\mathbb{W} \in [-L, L]^{n \times n}$, generated according to (2.1), in which $\mathcal{W} = \mathbb{Z}^* \Omega \mathbb{Z}^{*\top}$ and $\Omega \in \mathcal{F}_\alpha$, if $h \asymp 2\delta + \left(\frac{n_{max}\sqrt{d_0}}{\sqrt{\log n}}\right)^{\frac{2}{2\alpha+1}}$, the mean absolute spectral-norm error loss

$$\mathbb{E}_{\mathbb{Z}^*} \|B_h(\mathbb{W}) - \mathcal{W}\| \lesssim \max \left\{ \left(n_{max}^{\frac{1}{2\alpha+1}} (\log n)^{\frac{\alpha}{2\alpha+1}} \right), \log n \right\}$$

More specifically,

$$\mathbb{E}_{\mathbb{Z}^*} \|B_h(\mathbb{W}) - \mathcal{W}\| \lesssim \begin{cases} \left(n_{max}^{\frac{1}{2\alpha+1}} (\log n)^{\frac{\alpha}{2\alpha+1}} \right) & \text{if } n_{max} \gtrsim (\log n)^{\alpha+1} \\ \log n & \text{otherwise} \end{cases}$$

Theorem 3.1 explicitly shows the benefit of banding in reducing the mean absolute spectral-norm error loss under the scenario $n_{max} \gtrsim (\log n)^{\alpha+1}$, whose upper bound even keeps track of the interactions of several key model parameters (n, n_{max}, α) . The optimal banding parameter is reflective of the decay rate in the sense that a smaller α yields a larger h . On the contrary, for a finely-sliced network ($n_{max} = o((\log n)^{\alpha+1})$), banding seems to be not helpful since the mean absolute spectral-norm error loss is dominated by $\log n$ term.

Theorem 3.2 (mis-clustered error rate). Consider a sequence of similarity matrices $\mathbb{W}^1, \dots, \mathbb{W}^m$, generated independently according to (2.1) $\mathcal{W}^s = \mathbb{Z}^* \Omega^s \mathbb{Z}^{*\top}$ where $\Omega^s \in \mathcal{F}_{\alpha_s}$ defined in (2.2), and $\gamma_n^s = \gamma_n(\mathcal{W}^s)$. Given a weight vector λ , let \mathcal{M}_λ be the set of mis-clustered nodes given in Definition 1, then with probability at least $1 - m/n$,

$$\frac{|\mathcal{M}_\lambda|}{n} = O_p \left(\frac{n_{max}}{n} \sum_{s=1}^m \left(\frac{\lambda_s}{\gamma_n^s} \right)^2 \max \left(n_{max}^{\frac{2}{2\alpha_s+1}} (\log n)^{\frac{2\alpha_s}{2\alpha_s+1}}, (\log n)^2 \right) \right)$$

Corollary 3.1. Suppose $\Omega_1, \dots, \Omega_m \in \mathcal{F}_\alpha$ for some $\alpha > 0$, and $n_{\max} \asymp (\log n)^{\alpha+1}$, then with probability at least $1 - m/n$,

$$\frac{|\mathcal{M}_\lambda|}{n} = O_p \left(\frac{(\log n)^{\alpha+3}}{nn_{\min}^2} \right)$$

Furthermore, if the underlying \mathbb{Z}^* exhibits a balanced community structure, i.e., $n_{\max} \asymp n_{\min}$, then with probability at least $1 - m/n$,

$$\frac{|\mathcal{M}_\lambda|}{n} = O_p \left(\frac{1}{n(\log n)^{\alpha-1}} \right)$$

3.3 Optimal choice of $\{\lambda_s\}_{s=1}^m$

A remaining important question is that in what sense these m views can be optimally combined via the weighting parameters $\boldsymbol{\lambda} = (\lambda_1, \dots, \lambda_m)^\top$? Ideally, a desirable set of weight parameters $\boldsymbol{\lambda}^*$ shall minimize the population-level mis-clustered node size $\mathbb{E}_{\mathbb{Z}^*} |\mathcal{M}_\lambda|$ and thus can be referred as the oracle weight vector. Despite its attractiveness, an explicit form of $\mathbb{E}_{\mathbb{Z}^*} |\mathcal{M}_\lambda|$ is intractable due to the difficulty in deriving the deviation from $\widehat{\mathbb{U}}^s \widehat{\mathbb{U}}^{s\top}$ to $P_{\mathbb{Z}^*}$. As an alternative strategy, we seek to derive an upper bound of $\mathbb{E}_{\mathbb{Z}^*} |\mathcal{M}_\lambda|$ as a surrogate objective function, $q_h(\boldsymbol{\lambda})$, that leads to an approximately optimal solution that sufficiently reflects all m views. To this end, we note that from the proof of Theorem 3.2, $|\mathcal{M}_\lambda|$ is upper-bounded by $\|\sum_{s=1}^m \lambda_s \widehat{\mathbb{U}}^s \widehat{\mathbb{U}}^{s\top} - P_{\mathbb{Z}^*}\|^2$ up to a constant, and

$$\left\| \sum_{s=1}^m \lambda_s \widehat{\mathbb{U}}^s \widehat{\mathbb{U}}^{s\top} - P_{\mathbb{Z}^*} \right\|^2 \leq m \sum_{s=1}^m \lambda_s^2 \|\widehat{\mathbb{U}}^s \widehat{\mathbb{U}}^{s\top} - \mathbb{U}^s \mathbb{U}^{s\top}\|^2 \leq 4m \sum_{s=1}^m \left(\frac{\lambda_s}{\gamma_n^s} \right)^2 \|B_{h_s}(\mathbb{W}^s) - \mathcal{W}^s\|^2 \quad (3.4)$$

It thus suffices to derive an upper bound for each individual $\mathbb{E}_{\mathbb{Z}^*} \|B_{h_s}(\mathbb{W}^s) - \mathcal{W}^s\|^2$ as given below.

Theorem 3.3. Suppose $n_{\max} \gtrsim (\log n)^{\alpha_s+1}$, and choose $h_s = 2\delta + \left(\frac{Ln_{\max} \sqrt{d_0}}{\sqrt{\log n}} \right)^{\frac{2}{2\alpha_s+1}}$, $s = 1, \dots, m$, then for some constant $C > 0$,

$$\mathbb{E}_{\mathbb{Z}^*} \|B_{h_s}(\mathbb{W}^s) - \mathcal{W}^s\|^2 \leq Ch_s \sigma_s^2 \log n$$

and

$$\sum_{s=1}^m \left(\frac{\lambda_s}{\gamma_n^s} \right)^2 \|B_{h_s}(\mathbb{W}^s) - \mathcal{W}^s\|^2 \leq C \log n \sum_{s=1}^m \left(\frac{\lambda_s \sigma_s}{\gamma_n^s} \right)^2 h_s$$

Theorem 3.3 immediately implies that the surrogate objective function can be given as

$$q_{\mathbf{h}}(\boldsymbol{\lambda}) = \sum_{s=1}^m \left(\frac{\lambda_s \sigma_s}{\gamma_n^s} \right)^2 h_s \quad (3.5)$$

It is straightforward to see that $\boldsymbol{\lambda}_q^* = \operatorname{argmin}_{\boldsymbol{\lambda}: \sum_{s=1}^m \lambda_s = 1, \lambda_s \geq 0} q_{\mathbf{h}}(\boldsymbol{\lambda})$ takes the form

$$\lambda_{qs}^* = \left[h_s \left(\frac{\sigma_s}{\gamma_n^s} \right)^2 \sum_{t=1}^m h_t^{-1} \left(\frac{\gamma_n^t}{\sigma_t} \right)^2 \right]^{-1}, \quad s = 1, \dots, m. \quad (3.6)$$

Furthermore, if $\Omega_1, \dots, \Omega_m \in \mathcal{F}_\alpha$ for some common $\alpha > 0$,

$$\lambda_{qs}^* = \left[\left(\frac{\sigma_s}{\gamma_n^s} \right)^2 \sum_{l=1}^m \left(\frac{\gamma_n^l}{\sigma_s} \right)^2 \right]^{-1}, \quad s = 1, \dots, m. \quad (3.7)$$

It is easy to see from (3.7), $\lambda_s \propto (\gamma_n^s / \sigma_s)^2$, which can be comprehended as a measure of signal-to-noise ratio(SNR) since γ_n^s characterizes the capability of \mathcal{W}^s unveiling \mathbb{Z}^* at the population level whereas σ_s summarizes the sample-level (\mathbb{W}^s) corruption. This SNR flavored weighting scheme is seamlessly aligned with one's intuition that quality evaluation on each view shall consider its inherent ability and external noise extent simultaneously. To use it in practice, γ_n^s can be estimated by the largest K -th eigenvalue of $B_{h_s}(\mathbb{W}^s)$ and σ_s can be estimated as in Remark 3. More generally, (3.6) takes α_s into account through h_s^{-1} , which is also intuitive in the sense that it downweights the view with a slower decay rate. Although (3.7) is only a special case of (3.6), it is often the case in practice that α_s 's are very close or researchers prefer to take a bit more conservative perspective ($\alpha_1 \leq \alpha_2$ implies that $\mathcal{F}_{\alpha_2} \subseteq \mathcal{F}_{\alpha_1}$), in whichever case h_s makes negligible difference and (3.6) reduces to (3.7). In the sequel, we refer $\operatorname{mvBSC}_{\text{SNR}}$ to the mvBSC using (3.7) and mvBSC_q to the mvBSC using (3.6).

Remark 3 (Estimation of σ_s^2). *Recall that the variation in each similarity matrix consists of two sources: within group variation and across group variation. Let MSE_{within}^2 and MSE_{across}^2 denote the mean square error respectively. Given a membership matrix $\mathbb{Z} \in \mathcal{L}_{n,K}$,*

$$\begin{aligned} MSE_{\text{within}}^2 &= \sum_{k=1}^K \frac{1}{n_k(n_k - 1)/2 - 1} \sum_{\{(i,j): g_i = g_j = k, i < j\}} (W_{ij}^s - \hat{\Omega}_{kk}^s)^2 \\ MSE_{\text{across}}^2 &= \sum_{1 \leq k < l \leq K} \frac{1}{n_k n_l - 1} \sum_{\{(i,j): g_i = k, g_j = l\}} (W_{ij}^s - \hat{\Omega}_{kl}^s)^2 \end{aligned} \quad (3.8)$$

where $\hat{\Omega}_{kk}^s = \frac{2}{n_k(n_k-1)} \sum_{\{(i,j):g_i=g_j=k,i<j\}} W_{ij}^s$ and $\hat{\Omega}_{kl}^s = \frac{1}{n_k n_l} \sum_{\{(i,j):g_i=k,g_j=l\}} W_{ij}^s$.

Thus, σ_s^2 can be estimated by

$$\hat{\sigma}_s^2 = \frac{2}{K(K+1)} \left(MSE_{within}^2 + MSE_{across}^2 \right) \quad (3.9)$$

4 Simulations

We have performed extensive simulation studies to examine the finite sample clustering performance of the proposed mvBSC method. Throughout simulations, we let $m = 2$, $d(v_i, v_j) = |i - j|/10$ and use v_i and its index i exchangeably. To examine the robustness of mvBSC to the underlying network structure, we considered five different models (M1)-(M5) for the membership matrix \mathbb{Z}^* as illustrated in Figure 4.1 where nodes from the same cluster share the same color. In (M1), the clusters have a clear block structure with a total of 25 clusters and cluster size ranging from 9 to 28. Under (M1), our model assumption (C1) holds exactly with a small δ . We then gradually depart from this assumption by perturbing (M1). More specifically, for $k = 2, 3, 4, 5$, \mathbb{Z}^* in model (Mk) is generated by randomly swapping the node's membership in (M1) to one of the l_k most adjacent clusters with probability p_k , where we let $(p_2, l_2) = (0.01, 4)$, $(p_3, l_3) = (0.1, 2)$, $(p_4, l_4) = (0.05, 6)$ and $(p_5, l_5) = (0.1, 8)$. Thus p_k and l_k jointly control the degree of departure from assumption (C1) and the assumption no longer holds for a finite constant δ in the most challenging case of (M5). Throughout, we let $n = 500$ and for each membership model, we considered $K = 50, 25, 10$ to reflect a small, medium, large average cluster size.

For a given membership matrix \mathbb{Z}^* and its associated network partition $\mathcal{V} = \cup_{k=1}^K \mathcal{V}_k$, we let $c_k = \frac{1}{|\mathcal{V}_k|} \sum_{i:\mathbb{Z}_{ik}^*=1} i$ denote the centroid node of \mathcal{V}_k . We then generate each population level similarity matrix \mathcal{W}^s independently according to (2.1) from $\Omega^s \in \mathcal{F}_{\alpha_s}$ with $\alpha_1 = 0.4$ and $\alpha_2 = 0.6$, where

$$\Omega_{kl}^s = \begin{cases} 1 & \text{if } k = l \\ 0.6|c_k - c_l|^{-(\alpha_s+1)} & \text{if } k \neq l \end{cases} \quad (4.1)$$

The observed similarity matrix \mathbb{W}^s was generated as $W_{ij}^s = \{(\mathcal{W}_{ij}^s + \epsilon_{ij}^s) \wedge 1\} \vee (-1)$, where $\epsilon_{ij}^s \sim N(0, \sigma_s^2)$. We considered three noise levels with (σ_1, σ_2) being (i) (0.2, 0.4) for low noise; (ii) (0.4, 0.6) for median noise; and (iii) (0.6, 0.8) for high noise. Here, W_{ij}^s is thresholded to be between $[-1, 1]$

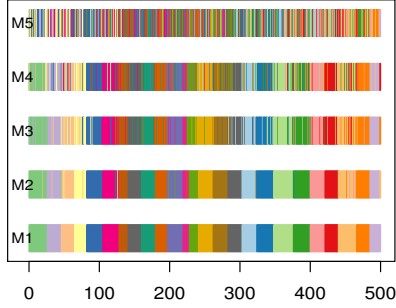


Figure 4.1: Graphical representation of the membership matrix \mathbb{Z}^* under (M1), (M2), (M3), (M4) and (M5) with groups indexed by colors.

to mimic the cosine similarity used in the real data example and we let all diagonals of \mathbb{W}^s to be 1. We choose $h_s = 2\delta + \left(\frac{Ln_{max}\sqrt{d_0}}{\sqrt{\log n}}\right)^{\frac{2}{2\alpha_s+1}}$, $s = 1, 2$ suggested in Theorem 3.3.

For each configuration, we performed clustering based on our proposed mvBSC method as well as a few existing methods including spectral clustering using (i) kernel addition (KA) matrix $\mathbb{W}^+ = \mathbb{W}^1 + \mathbb{W}^2$ (ii) the Laplacian of \mathbb{W}^+ (KAL); (iii) the normalized Laplacian of \mathbb{W}^+ (normKAL); (iv) each single \mathbb{W}^s alone (singleW); (v) the Laplacian of each single \mathbb{W}^s (singleL); and (vi) the normalized Laplacian of each single \mathbb{W}^s . Here, for a \mathbb{W} under consideration, the Laplacian matrix is derived using $\mathbb{W} - \min(\mathbb{W})$ since it is defined based on a non-negative adjacency matrix. For the mvBSC method, we considered different approaches to select λ including mvBSC $_q$ and mvBSC $_{SNR}$ as well as an oracle method that chooses λ by minimizing the mis-clustering rate. For each configuration and each clustering method, we quantify the quality of the clustering based on the average clustering accuracy, defined as one minus the mis-clustered error rate, and the normalized mutual information (NMI) over 100 replications. The NMI is a commonly used measure in the networks literature and is known to be impartial with respect to K (Strehl and Ghosh, 2002). Specifically, given a vertex set $\mathcal{V} = \{v_i\}_{i=1}^n$, the NMI between a partition \mathcal{X} with $\mathcal{V} = \mathcal{V}_1^{\mathcal{X}} \cup \dots \cup \mathcal{V}_{K_{\mathcal{X}}}^{\mathcal{X}}$ and a gold standard

reference partition \mathcal{X}_0 with $\mathcal{V} = \mathcal{V}_1^{\mathcal{X}_0} \cup \dots \cup \mathcal{V}_{K_{\mathcal{X}_0}}^{\mathcal{X}_0}$ is

$$\text{NMI}(\mathcal{X}, \mathcal{X}_0) = \frac{\sum_{k=1}^{K_{\mathcal{X}}} \sum_{l=1}^{K_{\mathcal{X}_0}} |\mathcal{V}_k^{\mathcal{X}} \cap \mathcal{V}_l^{\mathcal{X}_0}| \log \left(\frac{|\mathcal{V}_k^{\mathcal{X}} \cap \mathcal{V}_l^{\mathcal{X}_0}|}{|\mathcal{V}_k^{\mathcal{X}}| |\mathcal{V}_l^{\mathcal{X}_0}|} \right)}{\sqrt{\left\{ \sum_{k=1}^{K_{\mathcal{X}}} |\mathcal{V}_k^{\mathcal{X}}| \log \left(\frac{|\mathcal{V}_k^{\mathcal{X}}|}{n} \right) \right\} \left\{ \sum_{l=1}^{K_{\mathcal{X}_0}} |\mathcal{V}_l^{\mathcal{X}_0}| \log \left(\frac{|\mathcal{V}_l^{\mathcal{X}_0}|}{n} \right) \right\}}}, \quad (4.2)$$

which is a score ranging from 0 to 1 with a higher value indicating that \mathcal{X} is more similar to the reference partition \mathcal{X}_0 . We let \mathcal{X}_0 be the true underlying partition in our simulation studies and suppress the dependence on \mathcal{X}_0 for notation simplicity.

We first examine the effect of λ selection on the quality of the mvBSC clustering. Table 4.1 summarizes the mean and the standard deviation of the clustering accuracy and NMI score for the mvBSC clustering with λ selected via mvBSC_q, mvBSC_{SNR} and the oracle method under the five network structures (M1)–(M5) with $K = 25, \sigma_1 = 0.4, \sigma_2 = 0.6$. First, we note that both mvBSC_q and mvBSC_{SNR} have comparable clustering performance to that of the mvBSC trained with oracle λ across all settings. Although $\alpha_1 \neq \alpha_2$, selecting λ based on the simple mvBSC_{SNR} appears to result in clustering with near identical performance as that of mvBSC_q. These results suggest that the proposed procedure for selecting λ is indeed near optimal and the simple mvBSC_{SNR} works well when the views are reasonably similar.

We next compare the performance of mvBSC_q and mvBSC_{SNR} to the aforementioned alternative spectral clustering procedures. In Figure 4.2, we show the clustering accuracy and NMI for different clustering methods under (M3) with $K = 25$ and different noise levels for \mathbb{W}^s . For conciseness of the presentation, for the methods based on a single view, we only report the maximum accuracy and NMI of the two views. It is easy to see the normalized Laplacian always performs better than its unnormalized counterpart and in fact the unnormalized version fails in all scenarios. The KA clustering with \mathbb{W}^+ performs even worse than the clustering with the single view \mathbb{W}^s , suggesting that a naive aggregation of multiple sources of information could have detrimental effect on the clustering due to the heterogeneity in the underlying Ω^s . Our mvBSC method is consistently better than all competing methods in terms of both average and spread across all noise levels and the advantage is even more apparent as noise level increases. Figure 4.3 shows how the performances

model	method	Accuracy		NMI score	
		mean	sd	mean	sd
M1	oracle	0.966	0.0169	0.989	0.0046
	mvBSC _q	0.954	0.0255	0.985	0.0065
	mvBSC _{SNR}	0.952	0.0255	0.984	0.0068
M2	oracle	0.968	0.0145	0.988	0.0053
	mvBSC _q	0.945	0.0246	0.983	0.0061
	mvBSC _{SNR}	0.943	0.0272	0.983	0.0070
M3	oracle	0.968	0.0121	0.989	0.0036
	mvBSC _q	0.947	0.0248	0.984	0.0063
	mvBSC _{SNR}	0.947	0.0257	0.984	0.0065
M4	oracle	0.871	0.0272	0.948	0.0112
	mvBSC _q	0.826	0.0356	0.936	0.0100
	mvBSC _{SNR}	0.822	0.0367	0.936	0.0101
M5	oracle	0.734	0.0213	0.869	0.0156
	mvBSC _q	0.680	0.0344	0.857	0.0173
	mvBSC _{SNR}	0.671	0.0355	0.856	0.0182

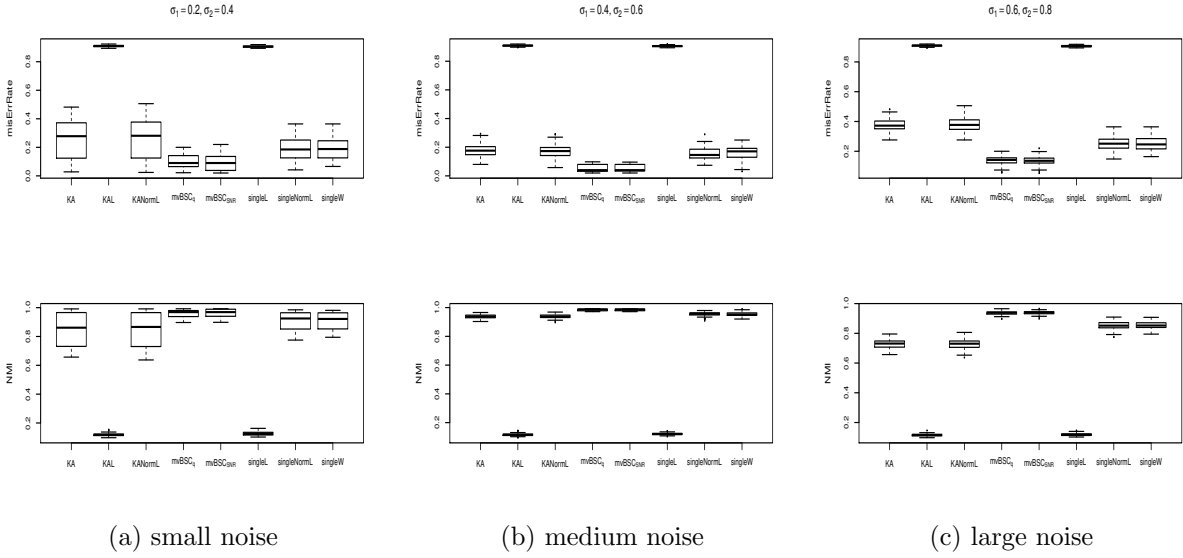
Table 4.1: The average clustering accuracy and NMI of mvBSC procedures under five different models with a medium noise level, $K = 25$ with optimal λ selected based on (3.6) (mvBSC_q), the empirical version of (3.7) (mvBSC_{SNR}) and the oracle obtained by minimizing the empirical $|\mathcal{M}_{\lambda^*}|$.

of different methods change over different level of K under the medium noise level setting. As K increases, the clustering becomes more challenging. As a result, the clustering accuracy and NMI decrease substantially for most competing methods but only slightly for the mvBSC method. Thus, the larger noise level and K , the more advantage the mvBSC approach showcases over other methods.

5 Grouping ICD9 Codes with mvBSC

5.1 Data Sources and Model Set-up

As discussed in the introduction section, it is of great interest to group ICD9 codes into clinically relevant ICD9 concept groups for clinical research studies. We aim to employ the proposed mvBSC algorithm to provide a data-driven grouping and contrast the results to the existing PheWAS grouping. To this end, we note that a typical ICD9 code consists of two parts with a three-digit number followed by one or two additional specifying digits. Take “427.31” as an example, its first three-digit “427” specifies cardiac arrhythmias and further digits are added to specify the type of



(a) small noise

(b) medium noise

(c) large noise

Figure 4.2: Boxplots of clustering accuracy and NMI of different clustering methods for (M3) with $K = 25$ and three different noise levels: (i) mvBSC_q: mvBSC using (3.6), (ii) mvBSC_{SNR}: mvBSC using (3.7), (iii) clustering using the kernel addition matrix \mathbb{W}^+ (KA); (iv) clustering with the Laplacian of the \mathbb{W}^+ (KAL); (v) clustering using the normalized Laplacian of \mathbb{W}^+ (normKAL); (vi) \mathbb{W}^1 (singleW), (vii) clustering with Laplacian of a single \mathbb{W} (singleL); and (viii) clustering with the normalized Laplacian of \mathbb{W}^1 .

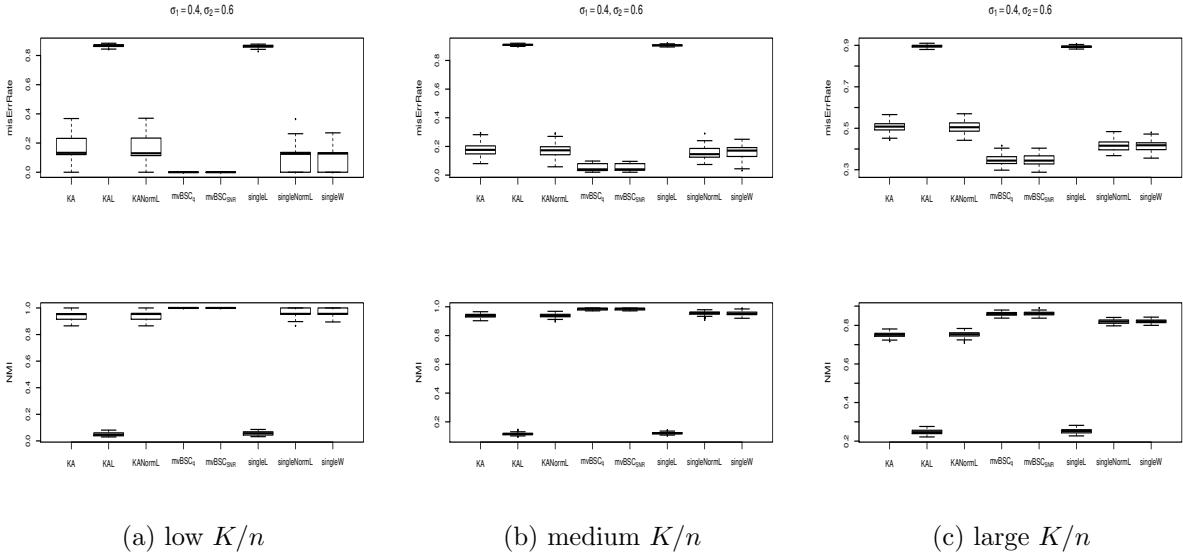


Figure 4.3: Boxplots of mis-clustered error rate and NMI score over multiple methods in comparison by three different K/n network structures. $mvBSC_q$: $mvBSC$ using (3.6), $mvBSC_{SNR}$: $mvBSC$ using (3.7), KA: the kernel addition matrix, KAL: Laplacian of the kernel addition matrix, normKAL: the normalized Laplacian of the kernel addition matrix, singleW: a single \mathbb{W} , singleL: Laplacian of a single \mathbb{W} , singleNormL: the normalized Laplacian of a single \mathbb{W} .

arrhythmias, in which case represents atrial fibrillation. In most cases, physicians are required to specify codes to the fourth or fifth digit to bill the patient’s insurance, although some diseases lack further specifications, e.g. 042, human immunodeficiency virus. ICD9 codes can be roughly grouped into 17 broad categories, simply based on their first three digits. For example, codes ranging from 001 to 139 are infectious and parasitic diseases while codes between 800 and 999 are injury and poisoning. In addition, the ICD9 system also incorporates special codes starting with E/V to include external causes of injury and supplemental classification. For illustration purposes, in this paper we only present results focusing on the following four categories—neoplasms, neurological, musculoskeletal and sense organs – whose grouping results draw particularly great interest in the current clinical studies.

To derive a data driven grouping, we obtained three similarity matrices $\{\mathbb{W}^s, s = 1, 2, 3\}$ for all ICD9 codes from three different healthcare systems including a large insurance claim database(Claim), the Veteran Health Administration (VHA) and Partner’s Healthcare systems (PHS). Here, W_{ij}^s rep-

represents the cosine similarity of the semantic vectors for ICD9 codes v_i and v_j from the sth data source. Within each healthcare system, the semantic vectors were obtained by fitting a *word2vec* algorithm (Mikolov et al., 2013 a) to a co-occurrence table that records the frequency of a code pair co-occurring within a 30-day time window. Two main factors contribute to the heterogeneity across the three data sources. First, the sample sizes are significantly different stretching from ~ 45 million for Claim down to 1 million for VHA and further reducing to $\sim 60,000$ for Partner’s Biobank. Second, the underlying patient populations vary substantially. Specifically, Claim covers a full nationwide spectrum of subjects, whereas VHA solely targets the veteran population and PHS primarily consists of tertiary hospitals enriched for patients with more complex and severe diseases. Such heterogeneities signify the need for an unbiased approach to optimally combine information from these sources, which can be also easily checked in Figure 5.1 that gives a summary of the raw data on the cosine similarity matrices. The top panel displays the density histogram of each cosine similarity matrix, which supports the sparseness in each cosine similarity matrix, even though the sparseness pattern in claim is not as apparent as the other two. The bottom panel is a snapshot of each cosine similarity matrix restricted on a common set of codes. The darkness of dots indicates the magnitude of the corresponding cosine similarity. Most large entries locate near the diagonal, suggesting the appropriateness of banding the three similarity matrices. For an ICD9 code v_i , we let $d_{ij} = |\mathcal{N}(v_i) - \mathcal{N}(v_j)| + \eta I\{v_i \neq v_j, \mathcal{N}(v_i) = \mathcal{N}(v_j)\}$, where $\mathcal{N}(\cdot)$ maps a character string to its numeric form and η is a small constant chosen such as 0.005. For example, $\mathcal{N}(\text{“001.1”}) = 1.1$. As a consequence, the vertex set \mathcal{V} can be ordered in the sense that $\mathcal{N}(v_i) < \mathcal{N}(v_j)$ if and only if $i < j$. The additional term involving a small constant η is included to distinguish the case of $v_i = v_j$ versus the rare cases when $\mathcal{N}(v_i) = \mathcal{N}(v_j)$ but $v_i \neq v_j$ (see for example Figure 5.2).

In this application, the existing manually curated PheWAS groups can also serve as silver-standard labels to provide a guidance in search for appropriate choices of the banding parameter h_s and the weight parameter λ_s . All parameters were tuned in a grid search manner with the best corresponding to the highest NMI score. To choose a proper K , considering the number of PheWAS groups(K_{phewas}) is already a good estimate, we scanned through its neighborhood ($0.8K_{phewas} \sim$

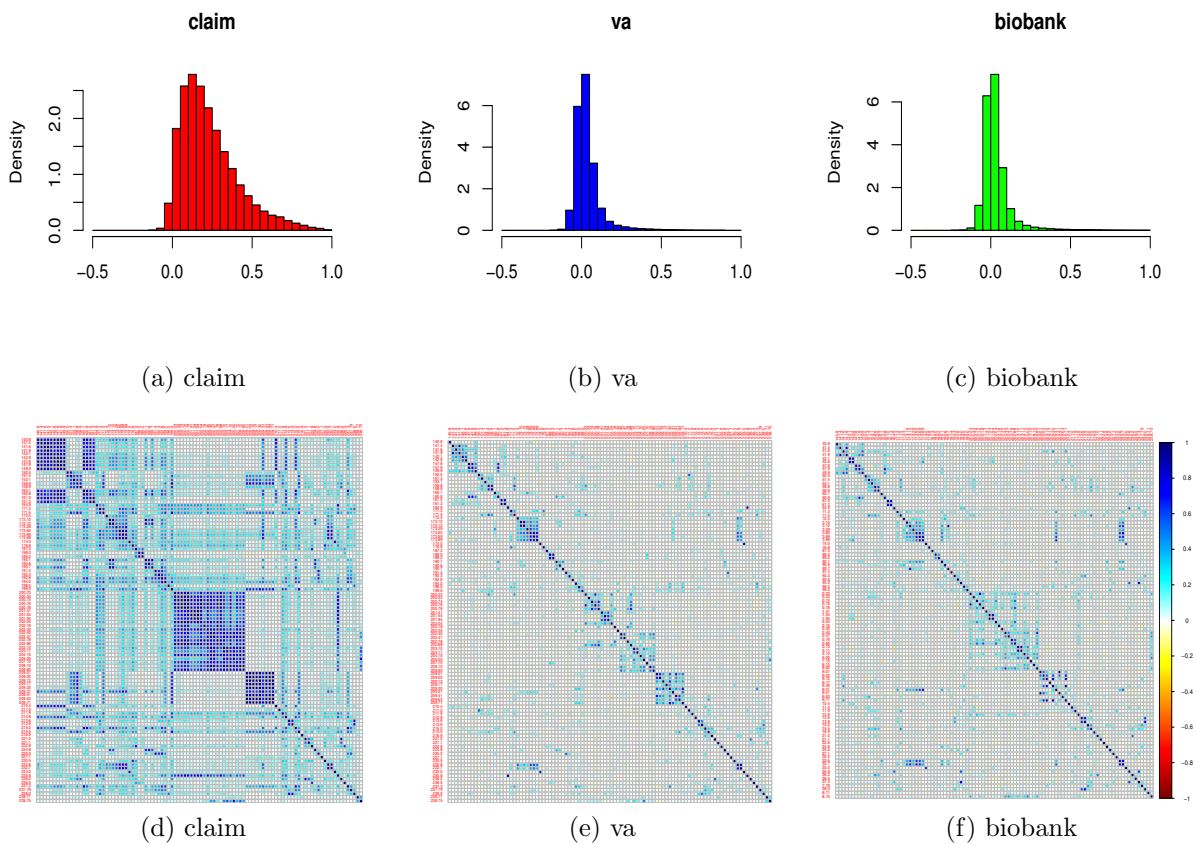


Figure 5.1: Raw data summary: the top panel displays the density histogram of each cosine similarity matrix. The bottom panel corresponds to each cosine similarity matrix restricted on a common set of codes.

```
##          ICD9                                ICD9.String
## 1:      010                                Primary tuberculous infection
## 2:    010.0                                Primary tuberculous infection
## 3: 010.00 Primary tuberculous infection, unspecified examination
```

Figure 5.2: Ambiguity example in ICD9 coding system

$1.2K_{phewas}$) and picked the one with the highest NMI score for subsequent analysis(K_{use}). With a given K , we performed clustering using the proposed $\text{mvBSC}_{\text{SNR}}$ procedure along with the mvBSC procedure with λ selected to empirically maximize the NMI ($\text{mvBSC}_{\text{maxNMI}}$). Results based on mvBSC_q are omitted here since three banding parameters are very close to each other which yield very similar results to $\text{mvBSC}_{\text{SNR}}$.

5.2 Results

Table 5.1 clearly shows that the proposed mvBSC algorithm performs well across four categories with high agreement with the existing PheWAS grouping. The clustering with λ selected via $\text{mvBSC}_{\text{SNR}}$ also has similar performance as the optimal λ selected to maximize the NMI. Figure 5.3 visually compares the the global clustering structure given by $\text{mvBSC}_{\text{SNR}}$ and PheWAS on neurological and musculoskeletal category respectively, showing the power of $\text{mvBSC}_{\text{SNR}}$ to mimic the global network structure.

Category	n	K_{phewas}	K_{use}	NMI score	
				$\text{mvBSC}_{\text{maxNMI}}$	$\text{mvBSC}_{\text{SNR}}$
neoplasms	799	122	138	0.856	0.843
neurological	364	68	56	0.852	0.839
musculoskeletal	675	124	128	0.834	0.790
sense organs	639	119	132	0.862	0.859

Table 5.1: Table of NMI scores of the mvBSC procedure compared to PheWAS labels using two different choices of λ (maximizing empirical NMI and SNR) across four different ICD categories, where n is the total number of ICD9 codes within each category, K_{phewas} is the total number of PheWAS groups and K_{use} is the total number of groups used for final clustering by maximizing the NMI score.

To further demonstrate its efficacy, we zoom in to individual three-digit categories of ICD9 codes and examine their grouping structures compared to PheWAS. Figure 5.4 shows a typical example that $\text{mvBSC}_{\text{SNR}}$ based grouping result perfectly agrees with PheWAS. In other cases, $\text{mvBSC}_{\text{SNR}}$ turns out to be quite robust with only a few occasional mismatches to the best grid results. For example Figure 5.5 compares the two corresponding results of category 368 in which only code 368.9 is grouped differently. Indeed $\text{mvBSC}_{\text{SNR}}$ seems to be able to do a better job in this scenario in that unspecified visual disturbance is clinically similar to any other specified disturbances and thus is

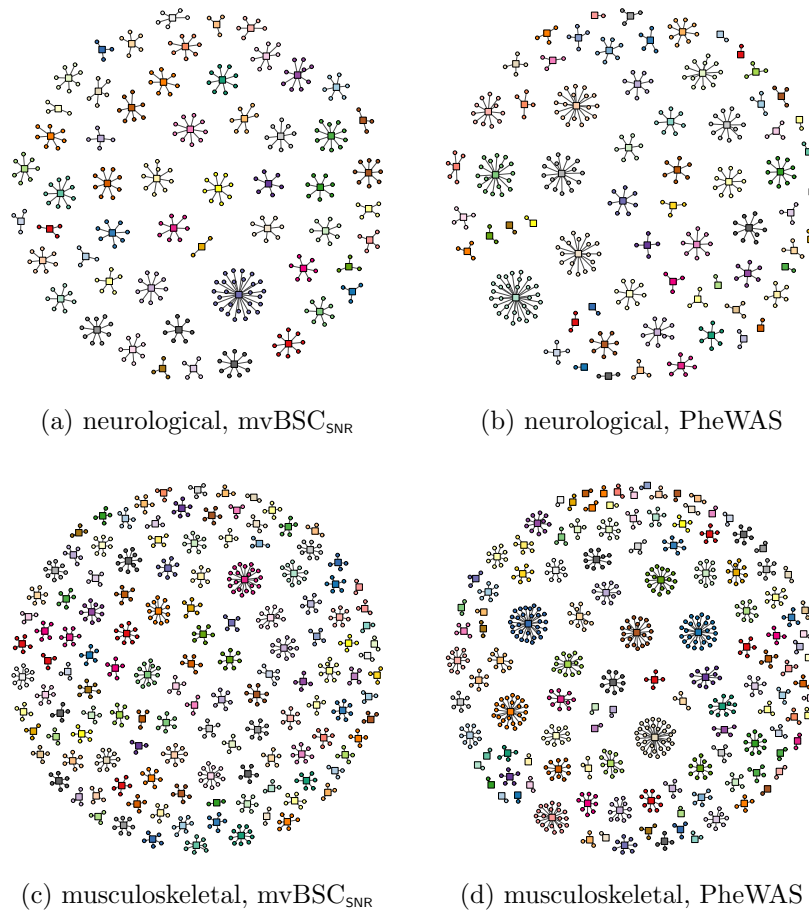


Figure 5.3: Clustering structure comparison. Squares represent cluster nodes and circles represent ICD9 codes.

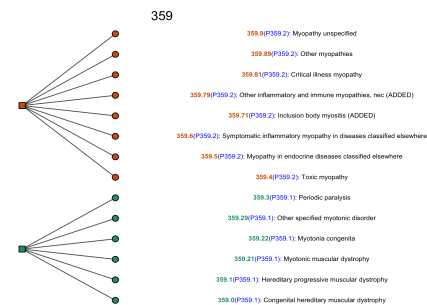


Figure 5.4: Grouping result for myopathy. Codes are colored by their membership. Codes in parenthesis colored in blue represent corresponding PheWAS codes.

not necessarily parsed out. Figure 5.6 (a) gives the clustering result on ICD9 codes starting with

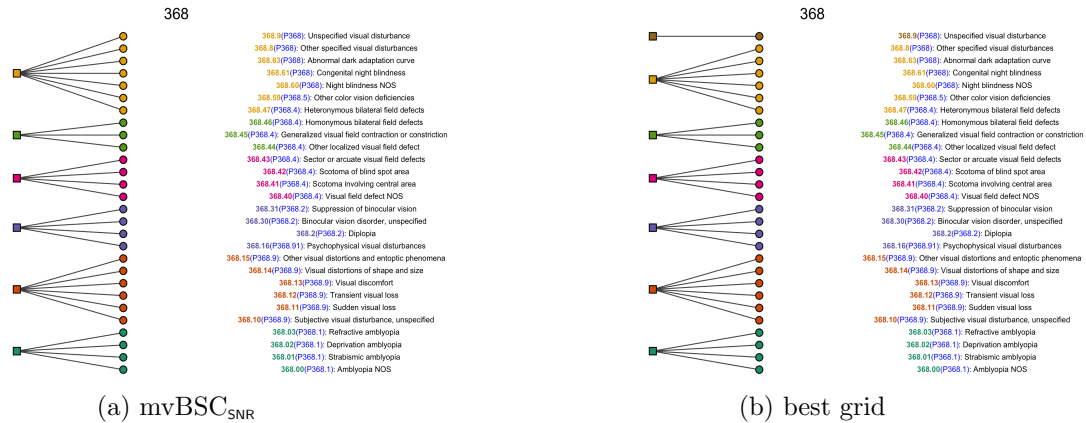


Figure 5.5: Grouping result for ICD9 . Codes are colored by their membership. Codes in parenthesis colored in blue represent corresponding PheWAS codes.

711. PheWAS separates these codes into four groups, with a majority of the codes being grouped to represent *Arthropathy associated with infections* (P711), followed by *Pyogenic arthritis* (P711.1), *Reiter’s disease* (P711.2), and *Behcet’s syndrome* (P711.3). On the other hand, $mvBSC_{SNR}$ separates these codes into seven concept groups with perfect agreement for codes in P711.1, P711.2 and P711.3. The main difference between $mvBSC_{SNR}$ grouping and PheWAS grouping appears in codes that belong to P711 by PheWAS. While our method does not distinguish postdysenteric arthropathy from arthropathy associated with viral and bacterial diseases, it can perfectly set apart anthropathy associated with unspecified infective arthritis, other infectious and parasitic diseases, and mycoses. As a final example, ICD9 codes starting with 714 consist of Rheumatoid Arthritis (RA) and Juvenile Rheumatoid Arthritis (JRA). Clinically, these are distinct diseases and thus should be grouped separately, despite adjacent coding representations and similar terminologies. Figure 5.6 (b) well demonstrates that our approach is able to distinguish between these two conditions.

6 Concluding remarks

In this paper, we introduce a novel multi-view spectral clustering ($mvBSC$) method for community detection of a network with ordered nodes. The novelty consists of two main parts. First, a consen-

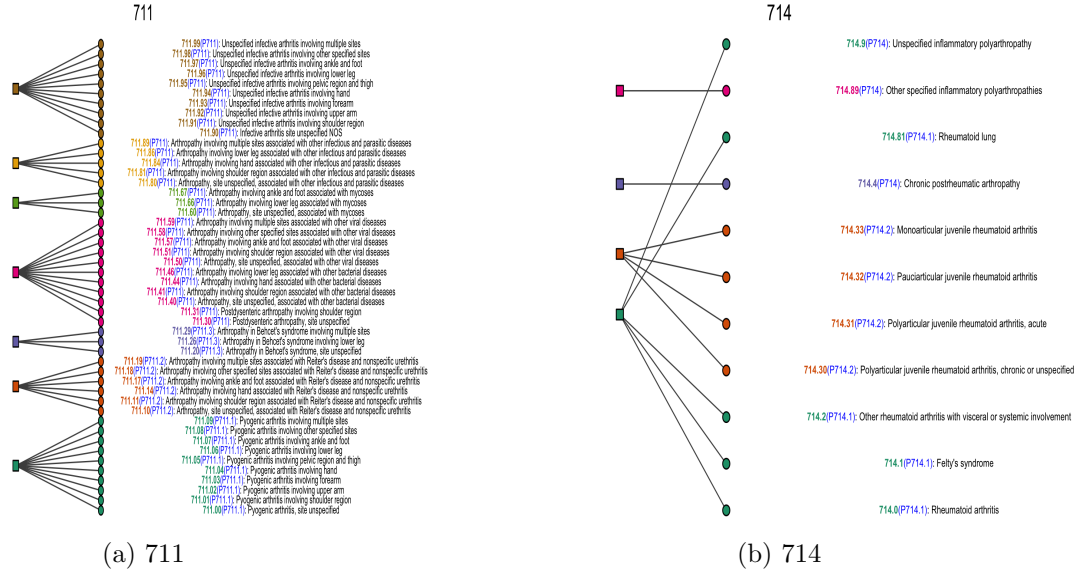


Figure 5.6: Grouping result for arthropathies. Codes are colored by their membership. Codes in parenthesis colored in blue represent corresponding PheWAS codes.

such clustering is realized by the means of a weighted sum of projector matrices that attempts to drag all views to a common ground while allowing for between view heterogeneity. Second, the proposed approach effectively leverages prior knowledge about the ordering of the nodes via the banding step, which essentially encourages a desired moving average clustering structure for the underlying network. The statistical performance of the proposed method is thoroughly studied under a multi-view stochastic block model (mvSBM) framework. In particular, we demonstrate the effect of a banding operation on reducing the error bound from \sqrt{n} to $\sqrt{\log n} \max\left(\sqrt{\log n}, \left(\frac{n_{max}}{\sqrt{\log n}}\right)^{\frac{1}{2\alpha_s+1}}\right)$ which shows explicitly the role of the decay parameter α_s in reducing the estimation error. Both simulations and the real data analysis demonstrate the effectiveness of the proposed mvBSC method to dramatically improve the clustering performance for a network with ordered nodes. We also provide a simple SNR based rule of choosing the weights that is intuitive and easy to follow in practice. However, we would like to make additional notes that this guideline may not yield a satisfactory result if a more complex heterogeneity pattern is present in the data. In this paper, we focus on the case where heterogeneity is only allowed across different views. Relaxing the homoscedasticity assumption within each view warrants further research.

References

- Asgari, E. and Mofrad, M. R. (2015), Continuous distributed representation of biological sequences for deep proteomics and genomics, *PloS one* **10**(11), e0141287.
- Bickel, P. J. and Chen, A. (2009), A nonparametric view of network models and newman–girvan and other modularities, *Proceedings of the National Academy of Sciences* **106**(50), 21068–21073.
- Bickel, P. J. and Levina, E. (2008), Regularized estimation of large covariance matrices, *The Annals of Statistics* pp. 199–227.
- Blaschko, M. B. and Lampert, C. H. (2008), Correlational spectral clustering, *in* ‘Computer Vision and Pattern Recognition, 2008. CVPR 2008. IEEE Conference on’, IEEE, pp. 1–8.
- Cai, X., Nie, F., Huang, H. and Kamangar, F. (2011), Heterogeneous image feature integration via multi-modal spectral clustering, *in* ‘Computer Vision and Pattern Recognition (CVPR), 2011 IEEE Conference on’, IEEE, pp. 1977–1984.
- Chaudhuri, K., Kakade, S. M., Livescu, K. and Sridharan, K. (2009), Multi-view clustering via canonical correlation analysis, *in* ‘Proceedings of the 26th annual international conference on machine learning’, ACM, pp. 129–136.
- Chen, R. Y., Gittens, A. and Tropp, J. A. (2012), The masked sample covariance estimator: an analysis using matrix concentration inequalities, *Information and Inference: A Journal of the IMA* **1**(1), 2–20.
- Choi, Y., Chiu, C. Y.-I. and Sontag, D. (2016), Learning low-dimensional representations of medical concepts, *AMIA Summits on Translational Science Proceedings* **2016**, 41.
- Denny, J. C., Bastarache, L., Ritchie, M. D., Carroll, R. J., Zink, R., Mosley, J. D., Field, J. R., Pulley, J. M., Ramirez, A. H., Bowton, E. et al. (2013), Systematic comparison of phenome-wide association study of electronic medical record data and genome-wide association study data, *Nature biotechnology* **31**(12), 1102–1111.

- Denny, J. C., Ritchie, M. D., Basford, M. A., Pulley, J. M., Bastarache, L., Brown-Gentry, K., Wang, D., Masys, D. R., Roden, D. M. and Crawford, D. C. (2010), Phewas: demonstrating the feasibility of a phenome-wide scan to discover gene–disease associations, *Bioinformatics* **26**(9), 1205–1210.
- Han, Q., Xu, K. S. and Airoidi, E. M. (2014), Consistent estimation of dynamic and multi-layer networks, *arXiv preprint arXiv:1410.8597*.
- Herzig, S. J., Howell, M. D., Ngo, L. H. and Marcantonio, E. R. (2009), Acid-suppressive medication use and the risk for hospital-acquired pneumonia, *Jama* **301**(20), 2120–2128.
- Holland, P. W., Laskey, K. B. and Leinhardt, S. (1983), Stochastic blockmodels: First steps, *Social networks* **5**(2), 109–137.
- Hurst, L. D., Pál, C. and Lercher, M. J. (2004), The evolutionary dynamics of eukaryotic gene order, *Nature Reviews Genetics* **5**(4), 299–310.
- Jin, J. et al. (2015), Fast community detection by score, *The Annals of Statistics* **43**(1), 57–89.
- Karrer, B. and Newman, M. E. (2011), Stochastic blockmodels and community structure in networks, *Physical Review E* **83**(1), 016107.
- Kiyota, Y., Schneeweiss, S., Glynn, R. J., Cannuscio, C. C., Avorn, J. and Solomon, D. H. (2004), Accuracy of medicare claims-based diagnosis of acute myocardial infarction: estimating positive predictive value on the basis of review of hospital records, *American heart journal* **148**(1), 99–104.
- Klompas, M., Haney, G., Church, D., Lazarus, R., Hou, X. and Platt, R. (2008), Automated identification of acute hepatitis b using electronic medical record data to facilitate public health surveillance, *PLOS one* **3**(7), e2626.
- Kumar, A. and Daumé, H. (2011), A co-training approach for multi-view spectral clustering, in ‘Proceedings of the 28th International Conference on Machine Learning (ICML-11)’, pp. 393–400.

- Lei, J., Rinaldo, A. et al. (2015), Consistency of spectral clustering in stochastic block models, *The Annals of Statistics* **43**(1), 215–237.
- Mikolov, T., Chen, K., Corrado, G. and Dean, J. (2013 a), Efficient estimation of word representations in vector space, *arXiv preprint arXiv:1301.3781* .
- Newman, M. E. (2006), Modularity and community structure in networks, *Proceedings of the national academy of sciences* **103**(23), 8577–8582.
- Ng, A. Y., Jordan, M. I. and Weiss, Y. (2002), On spectral clustering: Analysis and an algorithm, in ‘Advances in neural information processing systems’, pp. 849–856.
- Ng, P. (2017), dna2vec: Consistent vector representations of variable-length k-mers, *arXiv preprint arXiv:1701.06279* .
- Nguyen, D., Luo, W., Phung, D. and Venkatesh, S. (2016), Control matching via discharge code sequences, *arXiv preprint arXiv:1612.01812* .
- Paul, S., Chen, Y. et al. (2016), Consistent community detection in multi-relational data through restricted multi-layer stochastic blockmodel, *Electronic Journal of Statistics* **10**(2), 3807–3870.
- Qin, T. and Rohe, K. (2013), Regularized spectral clustering under the degree-corrected stochastic blockmodel, in ‘Advances in Neural Information Processing Systems’, pp. 3120–3128.
- Rohe, K., Chatterjee, S., Yu, B. et al. (2011), Spectral clustering and the high-dimensional stochastic blockmodel, *The Annals of Statistics* **39**(4), 1878–1915.
- Shi, J. and Malik, J. (2000), Normalized cuts and image segmentation, *IEEE Transactions on pattern analysis and machine intelligence* **22**(8), 888–905.
- Steinhaus, H. (1956), Sur la division des corp materiels en parties, *Bull. Acad. Polon. Sci* **1**(804), 801.
- Strehl, A. and Ghosh, J. (2002), Cluster ensembles—a knowledge reuse framework for combining multiple partitions, *Journal of machine learning research* **3**(Dec), 583–617.

Tropp, J. A. et al. (2015), An introduction to matrix concentration inequalities, *Foundations and Trends® in Machine Learning* **8**(1-2), 1–230.

Vu, V. Q., Lei, J. et al. (2013), Minimax sparse principal subspace estimation in high dimensions, *The Annals of Statistics* **41**(6), 2905–2947.

Xia, R., Pan, Y., Du, L. and Yin, J. (2014), Robust multi-view spectral clustering via low-rank and sparse decomposition., *in* ‘AAAI’, pp. 2149–2155.

Zhao, Y., Levina, E., Zhu, J. et al. (2012), Consistency of community detection in networks under degree-corrected stochastic block models, *The Annals of Statistics* **40**(4), 2266–2292.

A Appendix

A.1 Proof for Lemma 2.1

Proof. $\forall h > 2\delta$, since $d(v_i, v_j) \leq d(v_i, v_{c_{g_i}}) + d(v_{c_{g_i}}, v_{c_{g_j}}) + d(v_j, v_{c_{g_j}}) \leq d(v_{c_{g_i}}, v_{c_{g_j}}) + 2\delta$, $d(v_i, v_j) > h$ implies $d(v_{c_{g_i}}, v_{c_{g_j}}) > h - 2\delta > 0$. Therefore, for any i , $\sum_j \{|\mathcal{W}_{ij}^s| : d(v_i, v_j) > h\} = \sum_j \{|\Omega_{g_i g_j}^s| : d(v_{c_{g_i}}, v_{c_{g_j}}) > h - 2\delta\} \leq n_{max} \sum_l \{|\Omega_{g_i l}^s| : d(v_{c_{g_i}}, v_{c_{g_j}}) > h - 2\delta\} \leq n_{max} L(h - 2\delta)^{-\alpha_s}$. It is easy to see that $n_{min}\beta \leq \gamma_K(\mathcal{W}^s) \leq \gamma_1(\mathcal{W}^s) \leq n_{max}/\beta$, which completes the proof. \square

A.2 Proof of Theorem 3.1

Proof. Let \mathbb{E}_{ij} denote the $n \times n$ indicator matrix whose (i, j) -th and (j, i) -th entry is 1 and 0 elsewhere, then

$$\begin{aligned} B_h(\mathbb{W}) - \mathcal{W} &= B_h(\mathbb{W}) - B_h(\mathcal{W}) + B_h(\mathcal{W}) - \mathcal{W} \\ &= \left(\sum_{\substack{1 \leq i < j \leq n \\ d(v_i, v_j) \leq h}} (\mathbb{W}_{ij} - \mathcal{W}_{ij}) \mathbb{E}_{ij} \right) + \text{diag}(\omega_0 - \mathcal{W}_{ii}) + B_h(\mathcal{W}) - \mathcal{W} \end{aligned} \quad (\text{A.1})$$

Obviously, $\|(\mathbb{W}_{ij} - \mathcal{W}_{ij}) \mathbb{E}_{ij}\| \leq 4L$, and $\{(\mathbb{W}_{ij} - \mathcal{W}_{ij}) \mathbb{E}_{ij}\}_{d(v_i, v_j) \leq h, 1 \leq i < j \leq n}$ is a sequence of independent random matrices, using the matrix Bernstein inequality given in Theorem 6.6.1 in Tropp et al.

(2015),

$$\mathbf{E}_{\mathbb{Z}^*} \|B_h(\mathbb{W}) - \mathscr{W}\| \leq \sqrt{2\zeta \log n} + Ln_{max}(h - 2\delta)^{-\alpha} + \frac{4L}{3} \log n + 2L \quad (\text{A.2})$$

where

$$\zeta = \left\| \sum_{\substack{1 \leq i < j \leq n \\ d(v_i, v_j) \leq h}} \mathbf{E}_{\mathbb{Z}^*} [(W_{ij} - \mathscr{W}_{ij}) \mathbb{E}_{ij}]^2 \right\| = 2\sigma^2 \lfloor h/d_0 \rfloor \leq 2\sigma^2 h/d_0.$$

To find a proper order of h , it is easy to see that

$$\begin{aligned} \mathbf{E}_{\mathbb{Z}^*} \|B_h(\mathbb{W}) - \mathscr{W}\| &\leq 2\sqrt{\sigma^2 \frac{h}{d_0} \log n} + Ln_{max}(h - 2\delta)^{-\alpha} + \text{terms not involving } h \\ &\leq 2\sqrt{\sigma^2 \frac{h - 2\delta}{d_0} \log n} + Ln_{max}(h - 2\delta)^{-\alpha} + \text{terms not involving } h \end{aligned} \quad (\text{A.3})$$

Setting $\sqrt{\frac{h-2\delta}{d_0} \log n} \asymp n_{max}(h - 2\delta)^{-\alpha}$ yields $h \asymp 2\delta + \left(\frac{n_{max}\sqrt{d_0}}{\sqrt{\log n}}\right)^{\frac{2}{2\alpha+1}}$, and

$$\begin{aligned} \mathbf{E}_{\mathbb{Z}^*} \|B_h(\mathbb{W}) - \mathscr{W}\| &\lesssim \max \left(\left(n_{max}^{\frac{1}{2\alpha+1}} (\log n)^{\frac{\alpha}{2\alpha+1}} \right), \log n \right) \\ &\lesssim \begin{cases} \left(n_{max}^{\frac{1}{2\alpha+1}} (\log n)^{\frac{\alpha}{2\alpha+1}} \right) & \text{if } n_{max} \gtrsim (\log n)^{\alpha+1} \\ \log n & \text{o.w.} \end{cases} \end{aligned} \quad (\text{A.4})$$

□

A.3 Proof of Theorem 3.2

Proof. Recall that $(\widehat{\mathbb{Z}}, \widehat{\mathbb{A}}) = \operatorname{argmin}_{\mathbb{Z} \in \mathscr{Z}_{n,K}, \mathbb{A} \in \mathscr{R}^{K \times K}} \left\| \widehat{\mathbb{U}}_{\lambda}^* - \mathbb{Z}\mathbb{A} \right\|_F^2$, thus

$$\|\widehat{\mathbb{Z}}\widehat{\mathbb{A}} - \mathbb{U}^*Q\|_F^2 \leq 2\|\widehat{\mathbb{Z}}\widehat{\mathbb{A}} - \widehat{\mathbb{U}}_{\lambda}^*\|_F^2 + 2\|\widehat{\mathbb{U}}_{\lambda}^* - \mathbb{U}^*Q\|_F^2 \leq 4\|\widehat{\mathbb{U}}_{\lambda}^* - \mathbb{U}^*Q\|_F^2$$

Denote $\sum_{s=1}^m \lambda_s \widehat{\mathbb{U}}^s \widehat{\mathbb{U}}^{s\top}$ by \mathbb{T}_{λ} . It follows from the results from Lei et al. (2015) that

$$\|\widehat{\mathbb{U}}_{\lambda}^* - \mathbb{U}^*Q\|_F^2 \leq 8K \|\mathbb{T}_{\lambda} - \mathbb{U}^* \mathbb{U}^{*\top}\|^2 \leq 8mK \sum_{s=1}^m \lambda_s^2 \|\widehat{\mathbb{U}}^s \widehat{\mathbb{U}}^{s\top} - \mathbb{U}^s \mathbb{U}^{s\top}\|^2 \quad (\text{A.5})$$

$$\text{and } \|(\mathbb{I} - \widehat{\mathbb{U}}^s \widehat{\mathbb{U}}^{s\top}) \mathbb{U}^s \mathbb{U}^{s\top}\| \leq 2 \frac{\|B_{h_s}(\mathbb{W}^s) - \mathscr{W}^s\|}{\gamma_n^s}$$

where \mathbb{I} is the identity matrix.

In addition, since $\|(\mathbb{I} - \widehat{\mathbb{U}}^s \widehat{\mathbb{U}}^{s\top}) \mathbb{U}^s \mathbb{U}^{s\top}\| = \|\widehat{\mathbb{U}}^s \widehat{\mathbb{U}}^{s\top} - \mathbb{U}^s \mathbb{U}^{s\top}\|$, we have

$$\|\widehat{\mathbb{U}}_{\lambda}^* - \mathbb{U}^*Q\|_F^2 \leq 32mK \sum_{s=1}^m \left(\frac{\lambda_s}{\gamma_n^s} \right)^2 \|B_{h_s}(\mathbb{W}^s) - \mathscr{W}^s\|^2. \quad (\text{A.6})$$

It follows that

$$\begin{aligned}
|\mathcal{M}_\lambda| &= \sum_{i \in \mathcal{M}_\lambda} 1 \leq 2n_{max} \sum_{i \in \mathcal{M}_\lambda} \|\widehat{\mathbb{A}}_{g_i} - U_i^* Q\|_2^2 \leq 2n_{max} \sum_{i=1}^n \|\widehat{\mathbb{A}}_i - U_i^* Q\|_2^2 \\
&= 2n_{max} \|\widehat{\mathbb{Z}}\widehat{\mathbb{A}} - \mathbb{U}^* Q\|_F^2 \leq 8n_{max} \|\widehat{\mathbb{U}}_\lambda^* - \mathbb{U}^* Q\|_F^2 \\
&\leq 256mn_{max} K \sum_{s=1}^m \left(\frac{\lambda_s}{\gamma_n^s} \right)^2 \|B_{h_s}(\mathbb{W}^s) - \mathcal{W}^s\|^2
\end{aligned} \tag{A.7}$$

Using Bernstein inequality given in Theorem 6.6.1 in Tropp et al. (2015), for all $t \geq 0$,

$$\begin{aligned}
\Pr(\|B_{h_s}(\mathbb{W}^s) - \mathcal{W}^s\| \geq t) &\leq n \exp \left\{ \frac{-t^2/2}{2\sigma_s^2 h_s/d_0 + 4Lt/3} \right\} \leq \exp \left\{ \log n - \frac{t^2/4}{b_s(h_s + t)} \right\} \\
&\leq \begin{cases} \exp \left\{ \log n - \frac{t^2}{8b_s h_s} \right\} & \text{if } t \leq h_s \\ \exp \left\{ \log n - \frac{t}{8b_s} \right\} & \text{if } t \geq h_s \end{cases}
\end{aligned} \tag{A.8}$$

where $b_s = \max(\sigma_s^2/d_0, 2L/3)$. Hence, for any $r > 0$, with probability at least $1 - n^{-r}$,

$$\|B_{h_s}(\mathbb{W}^s) - \mathcal{W}^s\| \leq \begin{cases} c_s(r+1) \left(n_{max}^{\frac{1}{2\alpha_s+1}} (\log n)^{\frac{\alpha_s}{2\alpha_s+1}} \right) & \text{if } n_{max} \gtrsim (\log n)^{\alpha_s+1} \\ c_s(r+1) \log n & \text{o.w.} \end{cases} \tag{A.9}$$

for some positive constant c_s that depends on b_s . Applying the union bound, for any $r > 0$, with probability at least $1 - mn^{-r}$,

$$\|\widehat{\mathbb{U}}_\lambda^* - \mathbb{U}^* Q\|_F^2 \leq 32mK(r+1)^2 \sum_{s=1}^m \left(\frac{\lambda_s c_s}{\gamma_n^s} \right)^2 \max \left(n_{max}^{\frac{2}{2\alpha_s+1}} (\log n)^{\frac{2\alpha_s}{2\alpha_s+1}}, (\log n)^2 \right) \tag{A.10}$$

Therefore, dropping some constant terms not involving with n , with probability at least $1 - m/n$,

$$\frac{|\mathcal{M}|}{n} = O_p \left(\frac{n_{max}}{n} \sum_{s=1}^m \left(\frac{\lambda_s}{\gamma_n^s} \right)^2 \max \left(n_{max}^{\frac{2}{2\alpha_s+1}} (\log n)^{\frac{2\alpha_s}{2\alpha_s+1}}, (\log n)^2 \right) \right) \tag{A.11}$$

□

A.4 Proof of Corollary 3.1

Proof. Recall that γ_n^s is the K -th largest eigenvalue of \mathcal{W}^s , from Lemma 2.1, γ_n^s is at least at the scale of n_{min} . The results are natural simplifications of (A.11). □

A.5 Proof of Theorem 3.3

Proof. Recall that

$$\begin{aligned} \left\| \sum_{s=1}^m \lambda_s \widehat{\mathbf{U}}^s \widehat{\mathbf{U}}^{s\top} - \mathbf{U}^* \mathbf{U}^{*\top} \right\|^2 &\leq m \sum_{s=1}^m \lambda_s^2 \|\widehat{\mathbf{U}}^s \widehat{\mathbf{U}}^{s\top} - \mathbf{U}^s \mathbf{U}^{s\top}\|^2 \\ &\leq 4m \sum_{s=1}^m \left(\frac{\lambda_s}{\gamma_n^s} \right)^2 \|B_{h_s}(\mathbb{W}^s) - \mathcal{W}^s\|^2 \end{aligned} \quad (\text{A.12})$$

From (A.1),

$$\|B_{h_s}(\mathbb{W}^s) - \mathcal{W}^s\|^2 \leq 3(2L)^2 + 3(Ln_{\max}(h_s - 2\delta)^{-\alpha_s})^2 + 3 \left\| \sum_{\substack{1 \leq i < j \leq n \\ d(v_i, v_j) \leq h_s}} (\mathbb{W}_{ij}^s - \mathcal{W}_{ij}^s) \mathbb{E}_{ij} \right\|^2 \quad (\text{A.13})$$

Using Matrix second-moment inequality given in Chen et al. (2012),

$$\begin{aligned} \mathbb{E}_{\mathbb{Z}^*} \left\| \sum_{\substack{1 \leq i < j \leq n \\ d(v_i, v_j) \leq h_s}} (\mathbb{W}_{ij}^s - \mathcal{W}_{ij}^s) \mathbb{E}_{ij} \right\|^2 &\leq \left(2\sqrt{e \log n} \sqrt{\sigma_s^2 h_s / d_0} + 4e\sigma_s \log n \right)^2 \\ &= 4\sigma_s^2 e \log n \left(\sqrt{h_s / d_0} + 2\sqrt{e \log n} \right)^2 \\ &\leq 8\sigma_s^2 (h_s / d_0 + 4e \log n) e \log n \end{aligned} \quad (\text{A.14})$$

Setting $2\sqrt{\frac{h_s - 2\delta}{d_0} \log n} = Ln_{\max}(h_s - 2\delta)^{-\alpha_s}$,

$$\mathbb{E}_{\mathbb{Z}^*} \|B_{h_s}(\mathbb{W}^s) - \mathcal{W}^s\|^2 \leq 12L^2 + 12\frac{h_s}{d_0} (1 + 2e\sigma_s^2) \log n + 96\sigma_s^2 e^2 (\log n)^2 \quad (\text{A.15})$$

and

$$\begin{aligned} \sum_{s=1}^m \left(\frac{\lambda_s}{\gamma_n^s} \right)^2 \|B_{h_s}(\mathbb{W}^s) - \mathcal{W}^s\|^2 &\leq \frac{12 \log n}{d_0} \sum_{s=1}^m \left(\frac{\lambda_s}{\gamma_n^s} \right)^2 (1 + 2e\sigma_s^2) h_s + 96(e \log n)^2 \sum_{s=1}^m \left(\frac{\sigma_s \lambda_s}{\gamma_n^s} \right)^2 \\ &\quad + 12L^2 \sum_{s=1}^m \left(\frac{\lambda_s}{\gamma_n^s} \right)^2 \end{aligned}$$

Since $n_{\max} \gtrsim (\log n)^{\alpha_s + 1}$, $h_s \gtrsim \log n$, $s = 1, \dots, m$. Dropping some negligible and constant terms, we have

$$\mathbb{E}_{\mathbb{Z}^*} \|B_{h_s}(\mathbb{W}^s) - \mathcal{W}^s\|^2 \leq Ch_s \sigma_s^2 \log n$$

and

$$\sum_{s=1}^m \left(\frac{\lambda_s}{\gamma_n^s} \right)^2 \mathbb{E}_{Z^*} \|B_{h_s}(\mathbb{W}^s) - \mathcal{W}^s\|^2 \leq C \log n \sum_{s=1}^m \left(\frac{\sigma_s \lambda_s}{\gamma_n^s} \right)^2 h_s$$

□